TRANSNAV
http://www.transnav.eu
the International Journal
on Marine Navigation
and Safety of Sea Transportation
Volume 17
Number 1
March 2023
DOI: 10.12716/1001.17.01.02

A PPP Baseline Approach for Bridge Passing

C. Lass
German Aerospace Center (DLR), Neustrelitz, Germany

ABSTRACT: Global Navigation Satellite Systems (GNSS) are increasingly used as the main source of Positioning, Navigation and Timing (PNT) information for inland water navigation. In order to enable automated driving and facilitate driver assistant functions, it becomes of crucial importance to ensure high reliability and accuracy of the GNSS-based navigation solution, especially in challenging environments. One challenging phase of inland waterway navigation is bridge passing which leads to non-line-of-sight (NLOS) effects such as multipath and loss of tracking.
This work presents a Precise Point Positioning (PPP) based algorithm in a two-antenna system where one antenna is at the bow and the other is at the stern. Additionally, gyroscope data from an IMU is used. In contrast to a separated position calculation of the two antennas, only one antenna position is estimated and the other is derived from the baseline between the antennas. This allows for accurate positioning even if one antenna does not receive any GNSS measurements.
The presented scheme is evaluated using real measurement data from an inland water scenario with multiple bridges. In comparison with a standard PPP scheme as well as an RTK algorithm, the presented approach shows clear advantages in challenging scenarios.

1 INTRODUCTION

The demand for precise positioning, i.e. 10 cm horizontal and vertical position accuracy, in inland water applications has been increasing due to requirements of driver assistance functions [1] and the ongoing development of autonomous vehicles. Here, Global Navigation Satellite Systems (GNSS) are mainly used for the provision of Positioning, Navigation and Timing (PNT) information. The two classical algorithms to achieve cm-level accuracy based on GNSS are Real-Time Kinematic (RTK) and Precise Point Positioning (PPP) [2]. RTK uses the code and phase observations of a reference station close to the user's position to build double differences of the observations between the receivers as well as the satellites to mitigate atmospheric delays and errors on the satellites' side such as their orbits and clocks.

PPP, on the other hand, only uses the observations from one receiver but requires precise satellite orbit and clock information as well as ways to mitigate the atmospheric delay, e.g. applying atmospheric products, estimating the delays or using the ionospheric-free linear combination of the observations. A more recent trend is PPP-RTK [3,4] which is based on PPP but uses real-time corrections based on a network of reference stations. Here, the broadcast satellite orbits, satellite clocks, code and phase biases as well as atmospheric delays are corrected. This allows for fixing the ambiguities as

integers and achieving precise positioning without the long convergence time of estimated float ambiguities.

However, inland water navigation poses severe challenges [5] on the positioning in scenarios such as passing a waterway lock or passing a bridge where line-of-sight to the satellites cannot be guaranteed. Several methods to handle these challenges have been proposed such as robust filtering [6] to downweight or exclude faulty observations affected by multipath, the use of a multi-antenna setup [7,8,9] to have more redundancy as well as being able to determine the attitude of the vessel, and sensor fusion [10] using the angular velocities of an Inertial Measurement Unit (IMU). Nonetheless, most of these methods will fail, i.e. cannot provide precise position continuously, if there are no GNSS observations for several epochs.

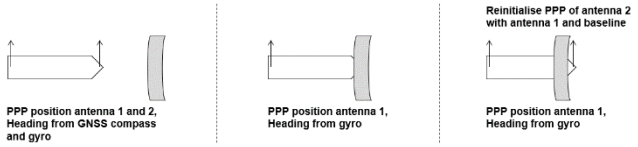

Figure 1. Bridge passing scheme using baseline approach

We propose a method which combines the approaches by using a multi-antenna setup and sensor fusion with an IMU based on PPP as well as applying moving baseline measurements in nominal conditions from an RTK approach between the antennas. The idea is to have two antennas on the vessel whose fixed baseline is longer than the width of the bridges and, ideally, orthogonal to the bridge crossed as can be seen in Figure 1. Then there is always at least one antenna which has line-of-sight to the satellites and a precise position. By knowing the pitch and yaw of the baseline with the help from previous baseline measurements and the angular velocities of an IMU, we can accurately determine the position of the other antenna. Due to this, as soon as the second antenna has line-of-sight again, we can quickly estimate the new ambiguities which helps in having a precise position even when the first antenna loses track of the GNSS satellites. This enables having precise position, velocity and heading information during and after bridge passing.

We start by explaining the methodology of our baseline approach based on PPP using the classical ionospheric-free linear combination which we then expand to two antennas using IMU as well as baseline measurements. Afterwards we apply the method to a real-world scenario and highlight the advantages in a difficult scenario for inland waterways, i.e. bridge passing, in comparison to the classical approach only using one antenna. In the end, we sum up the paper and show possible way forwards.

2 METHODS

We start with describing the classic PPP approach for one antenna where the unknowns are estimated in an Extended Kalman Filter (EKF) [11]. We apply the standard notation for Kalman Filters, i.e. F is used for the state-transition model, *X* for the Kalman state and h denotes the measurement functions.

To get precise results, we need precise satellite clock and orbits. For this, one can use postprocessed final products from the International GNSS Service (IGS) or the German Research Centre for Geosciences (GFZ). For real-time applications one can use global correction services such as the Galileo High Accuracy Service (HAS) [12] for GPS and Galileo satellite orbit, satellite clock, code and phase bias corrections, and the IGS Real-time Service [13] providing satellite clock, satellite orbit, code and phase bias corrections for GPS, GLONASS, Galileo, BeiDou as well as a global ionospheric model. Due to using the ionospheric-free linear combination, there is no need for local ionospheric corrections as required for PPP-RTK.

Hence, we assume precise satellite clock and orbits as well as the application of additional corrections for the Earth's tides and the phase center variation of the satellites.

2.1 *Problem formulation for one antenna*

In the following we consider two-frequency code $R_{i,1s}$ and phase observations $\Phi_{i,1s}$ where the frequency is denoted by i and the satellite by s

$$\begin{aligned} R_{i,1s} &= \|x_s - x_1\|_2 + c(\delta t_1 - \delta t_s) + T_{1s} + I_{i,1s} + \varepsilon_{i,1s} \\ \Phi_{i,1s} &= \|x_s - x_1\|_2 + c(\delta t_1 - \delta t_s) + T_{1s} - I_{i,1s} + \lambda_{i,s}(A_{i,1s} + w_{1s}) + \epsilon_{i,1s} \end{aligned} \quad (1)$$

The variables are the antenna position x_1, satellite position x_s, speed of light c, receiver clock offset δt_1, satellite clock offset δt_s, tropospheric delay T_{1s}, ionospheric delay $I_{i,1s}$, wave length $\lambda_{i,s}$, phase wind-up w_{1s}, integer ambiguity $A_{i,1s}$ and the remaining errors $\varepsilon_{i,1s}$, $\epsilon_{i,1s}$, e.g. multipath and receiver noise.

We then apply the classical ionospheric-free linear combination $(\cdot)_{IF}$ to (1) and split the tropospheric delay into the dry (Z_h) and the wet (Z_w) zenith delay. The zenith delays are used in conjunction with vienna mapping functions m_h, m_w [14] which depend on the elevation of the satellite, the receiver position and the time.

$$\begin{aligned} (\cdot)_{IF} &= \frac{f_1^2(\cdot)_1 - f_2^2(\cdot)_2}{f_1^2 - f_2^2} \\ (R)_{IF,1s} &= \|x_s - x_1\|_2 + c(\delta t_1 - \delta t_s) + T_{1s} + (\varepsilon_1)_{IF,s} \\ (\Phi)_{IF,1s} &= \|x_s - x_1\|_2 + c(\delta t_1 - \delta t_s) + T_{1s} + (\lambda A_1)_{IF,s} + (\lambda)_{IF,s} w_{1s} + (\epsilon_1)_{IF,s} \\ T_{1s} &= Z_{h,1} m_{h,1s} + Z_{w,1} m_{w,1s} \end{aligned} \quad (2)$$

The Kalman state X_1 consists of the antenna position x_1, velocity v_1, clock offsets $c\delta t_1$, clock drifts $c\dot{\delta} t_1$, the float ambiguities $(\lambda A_1)_{IF}$ and the wet zenith delay $Z_{w,1}$ whereas the dry zenith delay is approximated using the receiver's position. Assuming constant velocity and constant clock drifts for state transition and letting n_G being the number of GNSS and n_A the number of float ambiguities, this can be summarised as:

$$X_1^{t+\tau} = F(\tau)\cdot X_1^t = \begin{pmatrix} I_3 & \tau I_3 & & & & & \\ & I_3 & & & & & \\ & & I_{n_G} & \tau I_{n_G} & & & \\ & & & I_{n_G} & & & \\ & & & & 1 & & \\ & & & & & I_{n_A} & \end{pmatrix} \cdot \begin{pmatrix} x_1 \\ v_1 \\ c\delta t_1 \\ c\dot{\delta} t_1 \\ Z_{w,1} \\ (\lambda A_1)_{IF} \end{pmatrix}^t \quad (3)$$

To improve the a priori prediction for the position, velocity, receiver clock offsets as well as their drifts, we use time-differenced carrier phase measurements (TDCP) as described in [15]. This gives us highly accurate estimates of the change in position as well as change in the receiver clock offsets from the last to the current epoch which is especially important for real world scenarios where constant velocity cannot be assumed for all times.

The measurement functions for the code and phase observation of satellite s derived from (2) are

$$h_{1s}(X_1) = \begin{pmatrix} \|x_s - x_1\|_2 + c\delta t_1 + Z_{w,1} m_{w,1s} \\ \|x_s - x_1\|_2 + c\delta t_1 + Z_{w,1} m_{w,1s} + (\lambda A_1)_{IF,s} \end{pmatrix} \quad (4)$$

We use the Melbourne-Wübbena [16] and the geometry-free [17, p. 85-87] linear combination to detect cycle slips. In case a cycle slip is detected, the uncertainty of the respective float ambiguity is set to an arbitrary high value, e.g. 10^4, and the a priori ambiguity is estimated from the ionospheric-free linear combination of the phase observations and the a priori Kalman state.

2.2 *Two-antenna baseline approach*

The idea is that a second antenna is mounted on the vessel and we assume that the distance between the two antennas is constant. Then the position of the second antenna x_2 can be calculated using the position of antenna 1 and the baseline between the antennas, i.e.

$$x_2 = x_1 + C_{ENU}^{ECEF}(x_1)\cdot l(\theta,\psi) = \\ = x_1 + \begin{pmatrix} -\sin\lambda_1 & -\cos\lambda_1\sin\varphi_1 & \cos\lambda_1\cos\varphi_1 \\ \cos\lambda_1 & -\sin\lambda_1\sin\varphi_1 & \sin\lambda_1\cos\varphi_1 \\ 0 & \cos\varphi_1 & \sin\varphi_1 \end{pmatrix} \begin{pmatrix} \cos\theta\sin\psi \\ \cos\theta\cos\psi \\ \sin\theta \end{pmatrix} \|l\|_2 \quad (5)$$

$C_{ENU}^{ECEF}(x_1)$ is the transformation matrix from the ENU frame which has antenna 1 as its origin to an ECEF frame where φ_1 and λ_1 are the latitude and longitude of antenna 1. $l(\theta,\psi)$ is the baseline with θ and ψ being the pitch and yaw of the baseline which correspond to the elevation and azimuth of antenna 2 in the respective ENU frame. Both frames are displayed in Figure 2. As can be seen in (5) we only need to know the length of baseline but not how the antennas are mounted on the vessel, but ideally, they should be as far away as possible from front to back.

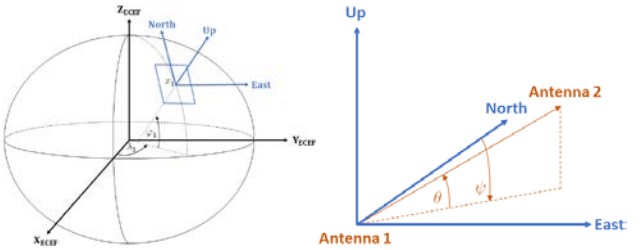

Figure 2. a) ENU in ECEF frame, b) ENU frame with antenna 1 in its origin

The velocity of antenna 2 can also be expressed in terms of antenna 1 and the baseline by totally differentiating (5) with respect to time:

$$v_2 = \frac{\mathrm{d}}{\mathrm{d}t} x_2$$

$$\underbrace{\dot{x}_1}_{\substack{\frac{\mathrm{d}}{\mathrm{d}t}\lambda(x_1)\approx 0 \\ \frac{\mathrm{d}}{\mathrm{d}t}\varphi(x_{1)\approx 0}}} v_1 + C_{ENU}^{ECEF}(x_1) \begin{pmatrix} -\sin\theta\sin\psi & \cos\theta\cos\psi \\ -\sin\theta\cos\psi & -\cos\theta\sin\psi \\ \cos\theta & 0 \end{pmatrix} \|l\|_2 \begin{pmatrix} \dot{\theta} \\ \dot{\psi} \end{pmatrix} \quad (6)$$

To link the rate of turn of the vessel with the change in the yaw of the baseline, we have to make some assumptions on the mounting of the antennas in the ship's body frame. Ideally, the baseline's projection onto the ship's horizontal plane, i.e. the plane defined by vessel's across and along ship axis as can be seen in Figure 3, is parallel to the along ship axis (Figure 3a) which would imply the pitch of the vessel differing from the pitch of the baseline in the ENU frame by a constant offset. Of course, for this we do need to know the height of the antennas in the ship's body frame. If the horizontal projection of the baseline is not parallel to the along ship axis, we have to assume the pitch of the baseline being identical to the pitch of the vessel, both with respect to the ENU frame. Hence, the baseline has to be parallel to the vessel's horizontal plane as displayed in Figure 3b. In both cases, the rate of turn of the ship would be identical to the change of the yaw of the baseline.

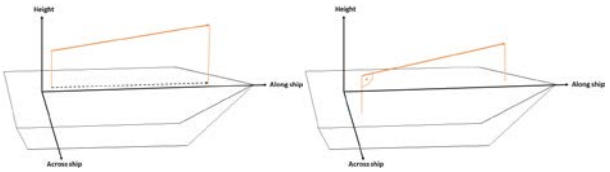

Figure 3. a) Baseline's horizontal projection, b) Baseline parallel to horizontal plane

To further reduce the number of parameters to be estimated, we assume the same wet zenith delay for both antennas, i.e. $Z_{w,1} = Z_{w,2} = Z_w$, since the length of the longest ships is less than half a kilometre. In practice, most ships are far shorter than that. All in all, the Kalman state for the second antenna only consists of the receiver clock offsets $c\delta t_2$, clock drifts $c\dot{\delta} t_2$ and the float ambiguities $(\lambda A_2)_{IF}$. Again, we assume constant receiver clock drifts.

$$X_2^{t+\tau} = F_2(\tau) \cdot X_2^t = \begin{pmatrix} I_{n_G} & \tau I_{n_G} & \\ & I_{n_G} & \\ & & I_{n_A} \end{pmatrix} \cdot \begin{pmatrix} c\delta t_2 \\ \dot{c}\delta t_2 \\ (\lambda A_2)_{IF} \end{pmatrix}^t \quad (7)$$

As with antenna 1, we use TDCP to get accurate estimates of the velocity and receiver clock drifts. Applying (6) gives us a measurement for v_1 whereas the change in the receiver clock offset of antenna 2 is used as an apriori estimate for its receiver clock drifts.

While the two-antenna baseline approach reduces the Kalman state for the second antenna, we have to estimate four additional parameters. These are the pitch θ and yaw ψ of the baseline as well as their velocities $\dot{\theta}$ and $\dot{\psi}$. Assuming constant angular velocity, the state-transition model for the baseline looks as follows:

$$X_{Base}^{t+\tau} = F_{Base}(\tau) \cdot X_{Base}^t = \begin{pmatrix} 1 & \tau & & \\ & 1 & & \\ & & 1 & \tau \\ & & & 1 \end{pmatrix} \cdot \begin{pmatrix} \theta \\ \dot{\theta} \\ \psi \\ \dot{\psi} \end{pmatrix}^t \quad (8)$$

To make further use of the two antennas, we apply a moving base approach as implemented in [18] to estimate the baseline whenever possible, i.e. we have enough good observations for the two antennas from the same satellites using double-differenced observations. The calculated baseline is then transformed from an ECEF into the ENU frame where its pitch and yaw can be determined. We use these two values as direct measurements of θ and ψ.

2.3 *IMU measurements*

The integration of an IMU requires considering additional measurements and parameters. The number of parameters depends on whether a full integration of all gyro as well as acceleration measurements is done or if a reduced model is chosen. We propose a simple model that only uses the biased rate of turn measurements.

In the following, we assume that the roll and pitch of the vessel as well as their velocities are 0 which is a fair assumption for large inland waterway vessels due to small waves and current as well as being less affected by smaller ships. Furthermore, the IMU is to be mounted on the vessel in such a way that each axis of the IMU is parallel to the respective axis of the vessel. By this, the rate of turn of the vessel is identical to the unbiased rate of turn of the IMU, and as described in section 2.2 identical to the change of yaw of the baseline.

All in all, the biased IMU measurements of the rate of turn can be described as

$$h_{IMU}(X) = \dot{\psi} + b_\psi \quad (9)$$

The gyro bias b_ψ is estimated in the Kalman Filter and is assumed to be constant, hence

$$X_{IMU}^{t+\tau} = F_{IMU}(\tau) \cdot X_{IMU}^t = 1 \cdot b_\psi^t \quad (10)$$

To make the pitch estimation more robust, we suggest to add an artificial angular velocity measurement of zero with regards to the pitch in case there is no baseline measurement. This is in line with our initial assumptions for the IMU on an inland waterway vessel. Using (3), (7), (8) and (10) the full Kalman state X of the two-antenna baseline approach and its transition model can be summarised as

$$X^{t+\tau} = F(\tau) \cdot X^t = \begin{pmatrix} F_1(\tau) & & & \\ & F_2(\tau) & & \\ & & F_{Base}(\tau) & \\ & & & F_{IMU}(\tau) \end{pmatrix} \cdot \begin{pmatrix} X_1 \\ X_2 \\ X_{Base} \\ X_{IMU} \end{pmatrix}^t \quad (11)$$

3 RESULTS

A measurement campaign was conducted on the 23rd of February 2022 in Strasbourg as part of the SCIPPPER project [19]. The goal was to automatically enter a waterway lock using GNSS, IMU as well as nearfield sensors. For this, we could use the Victor Hugo, a cruise ship from CroisiEurope. The dimensions of the vessel as well as the placement of the two geodetic antennas, each connected to a JAVAD Delta receiver, can be seen below:

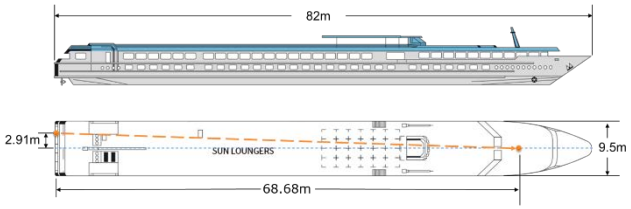

Figure 4. Schematic placement of the two GNSS antennas on the Victor Hugo

As displayed in Figure 4 the antennas were not mounted parallel to the ship's axes. Furthermore, the height of the antennas differed by 10 cm in the ship's body frame. In total, the length of the baseline was 68.74 metres and the displacement of the antennas caused an offset in the pitch and yaw of the baseline w.r.t. the ship's body frame of about 0.08° and 2.43° respectively. A sensonor MEMS IMU (STIM300) was mounted directly under the bow antenna. It has a gyro bias instability of 0.3 °/h and a gyro noise of 0.15 °/√h which were used in the Kalman Filter for the uncertainty of the gyro measurements as well as the uncertainty of the constant gyro bias assumption in the state-transition model.

To synchronise the GNSS observations with the IMU measurements which have a sampling rate of about 249 Hz, the IMU measurements are integrated over each epoch assuming piecewise constant values.

The ship started in the south in the harbour and drove northways crossing several bridges. After arriving at the waterway lock to the Rhine, it automatically entered the waterway lock three times from east to west [20]. Afterwards it went from north

to south back to the harbour, again crossing several bridges. The overall trajectory of the Victor Hugo and a nearby GNSS station are shown in the following figure:

Figure 5. Trajectory of Victor Hugo (black line) and GNSS station ENTZ00FRA (purple star) [Google Maps, 2022]

We use a postprocessed RTK solution from RTKLIB as a reference with the base station being the GNSS station ENTZ00FRA from the EUREF Permanent GNSS Network [21] as can be seen in Figure 5. During the measurement campaign the baseline between the base station and the antennas on the ship was between 10.5 and 12.5 kilometres long. A close-up of the ship's trajectory can later be seen in Figure 7.

We processed observations from GPS, GLONASS and Galileo with an elevation mask of 10° and a sampling rate of 2 Hz. The precise satellite clock and orbits were obtained from the final products of GFZ. The uncertainty of the state-transition model in the Kalman Filter was adapted to the Victor Hugo with the maximum acceleration in East and North assumed to be 0.5 m/s² and 0.1 m/s² in Up direction. The maximum angular acceleration for pitch and yaw was set to 0.1°/s². These uncertainties were observed as maximum values from measurements on previous days on the Victor Hugo and are therefore in general overbounds of the true uncertainties with regards to the ship's movement.

As a first proof of concept, we check whether the pitch and yaw of the PPP baseline approach converged to the correct values in a stationary scenario, even without IMU or baseline measurements. For this we look at a time when the vessel was in the harbour and the PPP algorithms were initialised at 8 a.m.

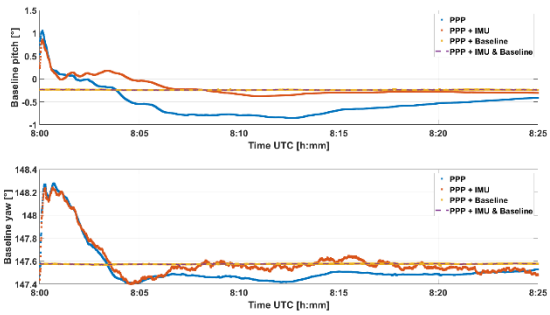

Figure 6. Pitch and yaw of the baseline in a stationary scenario

As can be seen in Figure 6 both pitch and yaw converged to the same values as the baseline measurements. When baseline measurements were included (yellow and purple line in the figure), the estimated values were almost identical to the measurements without needing to converge. Furthermore, including IMU measurements helped in determining the right pitch and yaw of the baseline faster. Without IMU measurements, it took about 31 and 14 minutes for pitch and yaw to be within 0.1° of the baseline measurements whereas with IMU measurements it only took about 14 and 6 minutes respectively.

Note that without baseline measurements the Kalman Filter needs reasonable approximations of the pitch and yaw as starting values to converge. We found that a single-differenced moving baseline approach only using code observations is good enough for this, so there is no need to apply advanced algorithms right from the start to resolve ambiguities.

Next, we have a look at the estimated heading during bridge passing. For this we mark five bridges passed during the measurement campaign which we will analyse in detail.

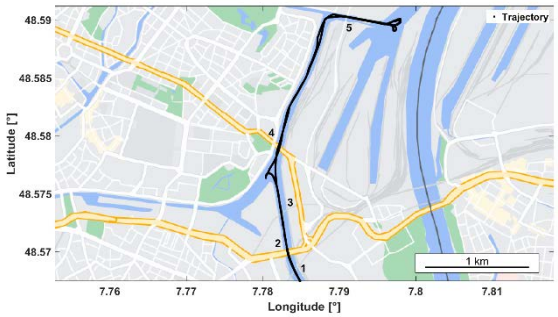

Figure 7. Five bridges that were passed during the measurement campaign [Google Maps, 2022]

Bridge 1 and 3 are railway bridges whereas bridge 2 (Pont Vauban), 4 (Pont d'Anvers) and 5 (Pont Pierre Brousse) can be crossed by cars. All bridges have a width of less than 25 metres which is shorter than half of the antennas' baseline on the Victor Hugo. In the following figure the estimated yaw with and without using IMU and/or baseline measurements during the passing of bridge 2 and 3 from south to north is shown.

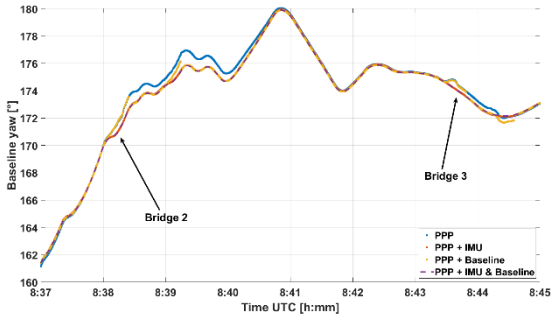

Figure 8. Yaw of baseline during passing of bridge 2 and 3

It is clear to see that without IMU measurements, the heading deviated when passing bridges by up to 1.3° since there is no yaw information if at least one

antenna has insufficient observations. During this time, there were no baseline measurements for 22 and 19 seconds respectively which is the time frame where the heading deviated by more than 0.1° (yellow line). Note that without IMU nor baseline measurements, it took about 3 minutes for bridge 2 (blue line) until the heading was correct again, i.e. within a range of 0.1°. When the IMU was used, the difference to the results using both IMU and baseline measurements was less than 0.07° the whole time, even without applying baseline measurements.

To sum it up, having consistent rate of turn information is crucial for our baseline approach during times when there are no baseline measurements which are important in nominal conditions to have precise pitch and yaw.

Next, we analyse the positioning results during the bridge passings. As we had no reference position during the passings, we took the positions of the RTK solution with fixed ambiguities closest to the respective bridge before and after the passing which were in agreement with the PPP baseline solution, i.e. within 10 cm in East and North. This is due to the RTK solution having some outliers close to bridges as displayed in Figure 9a. The straight line between those two points is our reference trajectory which is a reasonable approximation since all bridges were crossed without unnecessary turning. Furthermore, we assume constant velocity for the reference to analyse the along as well as the cross track error for the reference as seen in Figure 9b. Note that in the figure the grid lines of the along track axis coincide with the along track of the reference to better visualise deviations in this direction. Here, we compare the classic PPP approach for one antenna without any additional measurements as described in section 2.1 with our PPP baseline approach applying both IMU and baseline measurements. The following figure shows the positioning results of the stern antenna during the two time passing of Pont Pierre Brousse.

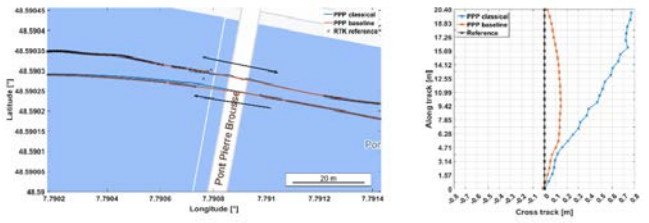

Figure 9. a) Passing bridge 5 two times, b) Cross and along track for East to West passage [Google Maps, 2022]

Both times our PPP baseline approach was better, i.e. the trajectory was straighter, than the classic approach. This is especially noticeable in the cross track direction when the vessel drove from east to west where the one antenna approach deviated to the north w.r.t. to the RTK reference after the bridge passing and it took about one minute until it was in agreement with the reference. During the passing from west to east there was no RTK solution for 36 seconds whereas the PPP baseline approach delivered reliable and precise results with regards to the reference line for all epochs.

A quantitative analysis for the different bridges can be found in Table 1. Here, classical stands for the one antenna approach and baseline denotes our baseline method. We computed the maximum absolute error as well as the root-mean-square error (RMSE) of the cross and along track error. We analysed the passings going from south to north for the first four bridges whereas we looked at the vessel driving from east to west for bridge 5 as can be seen in Figure 9b. To put the following numbers into perspective we also applied the analysis to an open sky scenario with a time frame of 15 seconds which occurred before the first passing of bridge 1. This was done to ensure that the classic PPP approach had converged and was not disturbed by previous NLOS events.

Table 1. Cross and along track error during bridge passings for stern antenna

	Cross track error [cm]				Along track error [cm]			
	Max		RMSE		Max		RMSE	
	C	B	C	B	C	B	C	B
Bridge 1, S→N	49.0	2.8	19.7	1.4	64.0	9.5	31.2	5.0
Bridge 2, S→N	77.1	26.6	42.8	17.7	87.9	12.0	42.6	3.8
Bridge 3, S→N	41.6	6.0	26.1	2.4	199.9	30.8	137.7	21.1
Bridge 4, S→N	56.8	19.0	37.2	11.3	21.8	7.3	12.1	4.3
Bridge 5, E→W	76.9	14.5	49.2	10.4	39.8	6.3	30.0	4.0
Open sky	5.8	4.9	2.7	3.2	11.6	9.4	6.0	5.9

C – Classical
B – Baseline

For all bridges our approach gave better results, even up to an order of magnitude as can be seen in the cross track error for bridge 1. Furthermore, the RMSE of the along track error was less or equal to 5 cm for four of the five bridges using our PPP algorithm which is remarkable for these difficult conditions where multipath and less observations would normally impact the quality of a GNSS based positing solution.

To highlight the non-line-of-sight (NLOS) effects of these scenarios we have a look at the number of visible satellites during the passing of Pont Vauban and the following railway bridge.

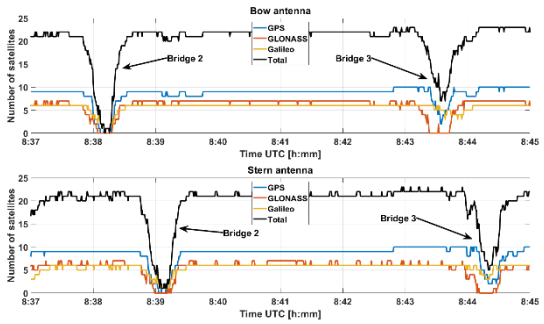

Figure 10. Number of visible satellites during passing of bridge 2 and 3 for the bow (top) and stern (bottom) antenna

Even though we used three GNSS, there were epochs without any observation for the stern antenna around 8:38 (UTC) which didn't have any major impact on the positioning using our baseline approach. During a time frame of 13 seconds, there were less than 6 satellites in view for both antennas during the first bridge passing. The spacial separation of the antennas can also be seen in the time difference between the minima of the visible satellites which is

about 45 seconds for the two antennas during the passing of the railway bridge. In nominal conditions each antenna had over 20 satellites in view with up to 10 from GPS and 6 to 7 satellites from each of Galileo and GLONASS.

Next, we analyse the position of the bow antenna. In Figure 11a we can see the RTK reference as well as the trajectory of both PPP algorithms for the passing of Pont Vauban from south to north.

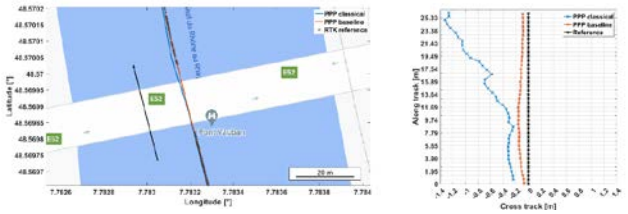

Figure 11. a) Passing bridge 2 from South to North, b) Cross and along track [Google Maps, 2022]

Again, the baseline approach gave superior results. Note that the classic approach deviated to the west during and after the passing where it converged to the RTK solution after some time. Additionally, in Figure 11b one can also see the errors along track especially before and after the passing of Pont Vauban. The baseline approach didn't have those large differences and was, apart from a slight offset to the west, in line with the RTK reference as well as the reference line which is defined in the same way as before. The quantitative results for the other bridges can be found in the following table. The additional open sky scenario refers to the same time frame as the one in Table 1.

Table 2. Cross and along track error during bridge passings for bow antenna

	Cross track error [cm]				Along track error [cm]			
	Max		RMSE		Max		RMSE	
	C	B	C	B	C	B	C	B
Bridge 1, S→N	93.1	18.0	39.2	14.8	275.1	15.5	238.5	10.8
Bridge 2, S→N	132.7	16.0	72.8	12.2	63.2	8.7	40.2	4.1
Bridge 3, S→N	60.9	7.4	26.9	3.9	36.7	10.3	16.8	4.1
Bridge 4, S→N	44.0	10.9	16.0	5.4	26.4	3.9	12.8	2.6
Bridge 5, E→W	26.9	10.9	12.1	7.6	26.4	10.4	15.6	7.0
Open sky	4.1	5.6	1.6	2.8	12.7	9.2	7.3	6.1

C – Classical
B – Baseline

Similar to the stern antenna, the PPP baseline approach yielded better results in all cases. Especially for bridge 2 where the along as well as the cross track error was almost an order of magnitude smaller with regards to the classic approach. Furthermore, the RMSE was below 10 cm in the majority of the bridge passings and 14.8 cm at most. This clearly shows the suitability of our approach for this difficult scenario.

4 CONCLUSIONS

We presented a PPP algorithm for two antennas based on the constant baseline length between them. By adding baseline as well as IMU measurements the algorithm is able to deliver precise and reliable positioning, even when one antenna suffers from non-line-of-sight effects. The method was applied to an inland waterway scenario and showed superior results with respect to the classic one antenna PPP approach, especially during the passing of bridges.

The algorithm could be improved if all IMU measurements were used as the additional acceleration measurements would be useful in determining the velocity. Furthermore, the integration of all angular velocities would be needed if the assumption of a constant pitch is not realistic due to waves from other ships or a strong current in general. Also, the approach can be generalised to any position on the baseline, e.g. in the middle of the baseline.

An additional improvement in the positioning results would be made possible by using undifferenced observations which have less noise than the ionospheric-free linear combination [17, p. 76]. On the one hand this would require additional estimation of or information on the atmospheric delays, but on the other hand this would allow for fixing the ambiguities as integers instead of just estimating them as float variables. This would allow for precise positioning with fast convergence. This becomes of upmost importance in the growing need for real-time application using PPP-RTK [4] and real-time correction services such as the Galileo High Accuracy Service [12] and the IGS Real-time Service [13].

ACKNOWLEDGEMENTS

This research was funded by the German Federal Ministry for Digital and Transport in the projects Digital SOW and AutonomSOW II as well as the German Federal Ministry for Economics and Climate Action (grant number 03SX470E) in the project SCIPPPER. We also want to thank CroisiEurope for allowing us to conduct the measurement campaign on the Victor Hugo.

REFERENCES

[1] A. Hesselbarth, D. Medina, R. Ziebold, M. Sandler, M. Hoppe, and M. Uhlemann, Enabling Assistance Functions for the Safe Navigation of Inland Waterways. IEEE Intelligent Transportation Systems Magazine 2020, 12, 123–135. https://doi.org/10.1109/MITS.2020.2994103

[2] J.F. Zumberge, M.B. Heflin, D.C. Jefferson, M.M. Watkins and F.H. Webb, Precise point positioning for the efficient and robust analysis of GPS data from large networks. Journal of Geophysical Research: Solid Earth 1997, 102, 5005–5017. https://doi.org/10.1029/96JB03860

[3] G. Wuebbena, M. Schmitz and A. Bagge, PPP-RTK: Precise Point Positioning Using State-Space Representation in RTK Networks. In Proceedings of the 18th International Technical Meeting of the Satellite Division of The Institute of Navigation (ION GNSS), 2005, pp. 2584 – 2594

[4] X. An, R. Ziebold and C. Lass, From RTK to PPP-RTK: towards real-time kinematic precise point positioning to support autonomous driving of inland waterway vessels. GPS Solutions 27, 86 (2023). https://doi.org/10.1007/s10291-023-01428-2

[5] I. Vierhaus, A. Born and D. Minkwitz, Challenges to PNT and driver assistance systems in inland water. In

Proceedings of the The 14th IAIN Congress 2012 Seamless Navigation (Challenges & Opportunities). IAIN, 2012, pp. 1–10
[6] D. Medina, H. Li, J. Vilà-Valls and P. Closas, Robust Filtering Techniques for RTK Positioning in Harsh Propagation Environments. Sensors 2021, 21. https://doi.org/10.3390/s21041250
[7] C. Lass, D. Medina, M. Romanovas, I. Herrera-Pinzón and R. Ziebold, Methods of Robust Snapshot Positioning in Multi-Antenna Systems for Inland water Applications. In Proceedings of the European Navigation Conference (ENC), 2016
[8] D. Medina, J. Vilà-Valls, A. Hesselbarth, R. Ziebold and J. García, On the Recursive Joint Position and Attitude Determination in Multi-Antenna GNSS Platforms. Remote Sensing 2020, 12. https://doi.org/10.3390/rs12121955
[9] T. Kersten, L. Ren and S. Schön, A Virtual Receiver Concept for Continuous GNSS based Navigation of Inland Vessels. In Proceedings of Navitec 2018, 5.-7. December 2018, Noordwijk, The Netherlands. https://doi.org/10.15488/3898
[10] R. Ziebold, M. Romanovas and L. Lanca, Evaluation of a Low Cost Tactical Grade MEMS IMU for Maritime Navigation. In Activities in Navigation; Weintritt, A., Ed.; Marine Navigation and Safety of Sea Transportation, CRC Press, 2015, pp. 237–246
[11] R.E. Kalman, A New Approach to Linear Filtering and Prediction Problems, Transactions of the ASME--Journal of Basic Engineering 1960, 82, pp. 35-45
[12] I. Fernandez-Hernandez, A. Chamorro-Moreno, S. Cancela-Diaz, J. Calle-Calle, P. Zoccarato, D. Blonski, T. Senni, F. Blas, C. Hernández, J. Simón and et al., Galileo high accuracy service: initial definition and performance. GPS Solutions 2022, 26. https://doi.org/10.1007/s10291-022-01247-x
[13] M. Caissy, L. Agrotis, G. Weber, M. Pajares and U. Hugentobler, The international GNSS real-time service. GPS World 2012, 23, pp. 52–58
[14] J. Boehm, and H. Schuh, Vienna Mapping Functions. In Proceedings of the Conference: 16th EVGA Working Meeting, 2003
[15] C. Lass, and R. Ziebold, Development of Precise Point Positioning Algorithm to Support Advanced Driver Assistant Functions for Inland Vessel Navigation. TransNav, the International Journal on Marine Navigation and Safety of Sea Transportation 2021, 15, 781–789. https://doi.org/10.12716/1001.15.04.09
[16] G. Blewitt, An Automatic Editing Algorithm for GPS data. Geophysical Research Letters 1990, 17, 199–202. https://doi.org/10.1029/GL017i003p00199
[17] J. Sanz Subirana, J.M. Juan Zornoza and M. Hernández-Pajares, GNSS Data Processing, Vol. I: Fundamentals and Algorithms; ESA Communications, 2013
[18] T. Takasu, and A. Yasuda, Development of the low-cost RTK-GPS receiver with an open source program package RTKLIB. In Proceedings of the International Symposium on GPS/GNSS, International Convention Center Jeju, Korea, 2009
[19] SCIPPPER. Schleusenassistenzsystem basierend auf PPP und VDES fuer die Binnenschifffahrt. http://scippper.de. [Accessed 04-October-2022]
[20] SCIPPPER. Schleusenassistenzsystem basierend auf PPP und VDES fuer die Binnenschifffahrt. https://www.youtube.com/watch?v=CFU7MZWXP8I. [Accessed 12-October-2022, from 09:19 onwards]
[21] C. Bruyninx, J. Legrand, A. Fabian, and et al., GNSS metadata and data validation in the EUREF Permanent Network. GPS Solutions 2022, 23, 106, 2019. https://doi.org/10.1007/s10291-019-0880-9